 CMES, vol.3, no.6, pp.773-789, 2002

# Computational Aeroelasticity Using a Pressure-based Solver

**Ramji Kamakoti[1], Yongsheng Lian[1], Sean Regisford[1], Andrew Kurdila[1] and Wei Shyy[1]**

**Abstract:** The non-linear fluid-structure interaction problem is studied for two different wing configurations based on moving grid techniques. These configurations demonstrate the interaction between a rigid structure and fluid, as well as the interaction between a flexible structure and fluid. A closely-coupled approach is used to perform the combined fluid and structure interaction computations. The flow solver is an unsteady, implicit, three-dimensional, multi-block, pressure-based Navier-Stokes solver. The structure solver for the AGARD wing model is based on a linear, time-invariant model derived via classical structural finite elements whereas the flexible structural solver is based on a non-linear dynamic membrane model with the material obeying the hyperelastic Mooney's model. Suitable interfacing techniques are incorporated to couple and synchronize the flow and structure solvers. We present unsteady computations performed on both rigid and membrane wings to highlight the computational characteristics.

## 1 Introduction

The interaction of aerodynamic forces and inertial forces within elastic structural systems is a well-known and difficult problem. In a coupled system, the external forces acting on a structural system such as a wing leads to a deformation in the wing geometry, and this structural deformation thereby leads to modified aerodynamic loads. While computational methods that study different aspects of aeroelastic response have been studied for some time, numerous open research issues remain to be resolved. For example, many approaches in computational aeroelasticity seek to synthesize independent computational approaches for the aerodynamic and the structural dynamic subsystems. This strategy is known to be fraught with complications associated with the interaction between the two simulation modules. Some of the issues arise from the fact that the computational fluid dynamic (CFD) and the computational structural dynamic (CSD) mesh systems are quite different. Frequently, the former uses a Eulerian or spatially fixed coordinate system while the latter uses a Lagrangian or material fixed coordinate system. Hence, care must be taken to develop a suitable interfacing technique between the two modules. Also, since the time scales are different for the two modules, synchronization of the flow and structure solvers are no longer straightforward.

Computational aeroelasticity (CAE) can be classified into two major classes. They are coupled analysis and uncoupled analysis. The coupled analysis can be further divided into fully coupled and closely-coupled analysis. In an uncoupled analysis, the fluid domain and structural system are treated as two separate modules with only external interaction between them. This method is limited to small perturbations with nominally linear structural models. In fully coupled analysis, the governing equations for fluids and structures part are combined into one set of equations and these equations are subsequently solved and integrated in time simultaneously. Since the matrices associated with structures are an order of magnitude stiffer than those associated with fluids, it is virtually impossible to solve the entire system using a monolithic numerical scheme. However, some methods have been developed using fully coupled methods, but are mainly restricted to 2-D problems. In the closely-coupled approach, the fluid domain and structural system are modeled in separate domains but they are unified into one module. The exchange of information between the fluid and structure modules takes place at the interface. The coupling is integrated thereby allowing efficient exchange information at the interface. Several models have been developed over the years to solve various problems in aeroelasticity addressing several issues discussed thus far. A few of them are discussed next.

Cunningham et al. (1988) developed a computational scheme for transonic aeroelastic analysis using the tran-

[1] Dept. of Mechanical and Aerospace Engineering
University of Florida
Gainsville, FL, USA

sonic small disturbance (TSD) formulation. The equations of motion were based on the natural vibrational modes of the aircraft. Robinson et al. (1991) developed a model along the same lines but made use of deforming mesh scheme for re-meshing the CFD domain. This technique of using TSD formulation fails when there is a strong shock or when viscous effects dominate. To overcome this, Schuster et al. (1990) came up with a model that used a 3-D flow solver coupled with a linear static structure model to study the aeroelastic analysis of a fighter aircraft. Grid deflection method was used to update the grid after each time step. This method was limited to static analysis. Lewis and Smith (1998) extended this method using shell finite element structures to study flutter in an engine liner.

Guruswamy and Byun (1993, 1995) developed a method by directly coupling Euler/Navier-Stokes equations for fluids with plate/shell finite element structures. A domain decomposition method, wherein fluids and structures modules were solved in separate modules, was used in this regard. The transformation of loads from CFD mesh to CSD mesh was done by bilinear interpolation and virtual surface methods. Bhardwaj et al. (1998) developed a coupling procedure that combined a variety of CFD and CSD codes. Patil et al. (1999, 2000) developed a theoretical as well as computational non-linear aeroelastic model for high aspect-ratio wings. They used the mixed variational formulation of beams in moving frames. Garcia and Guruswamy (1999) developed a coupled model of Navier-Stokes flow model with beam finite element model to perform static aeroelastic analysis of high aspect-ratio wings. Farhat and Lesoinne (2000) developed a serial as well as a parallel algorithm for nonlinear transient aeroelastic problems. They used the Arbitrary Lagrangian Eulerian (ALE) formulation with a deforming mesh algorithm for grid movement. On a similar note, Rugonyi and Bathe (2001) used a direct as well as partitioned solution procedure using the ALE formulation to solve fluid-structure interaction problems for incompressible flows. Soulaimani (2000) developed a FEM based solver for 3-D Euler and Navier-Stokes flow equation coupled with a commercial FEM code for nonlinear CAE. A brief summary of a few models explaining the salient features like the flow solver, structural solver used, etc and the test cases used to relate the models is presented in Table 1.

Our model makes use of the closely-coupled approach that synthesizes a multi-block 3-D CFD solver and a linear, time-invariant structural model. The CFD code addresses the full 3-D Navier-Stokes equations along with well-validated turbulence models. The solver also has the capability to include effects for multi-block moving boundary treatment. We use linear interpolation and extrapolation techniques to carry out the interfacing between the two modules. The motivation for this work is to expand our well-validated CFD approach to study coupled aeroelastic models and consider the complexity of coupling procedures in 3-D wing models.

The main objective of this work is to study the fluid-structure interaction problem for 3-D wing geometries. We consider the AGARD 445.6 wing (Yates, 1987) and a membrane wing motivated by micro-air vehicle applications (Ifju et al., 2002) to demonstrate our methodology. In this work, we focus on the meshed approach with moving grid techniques. It should be noted that recent development in meshless methods (for comprehensive reviews, see e.g., Atluri and Shen (2002a,b), and Li and Liu (2002)) has also been extended to treat flexible structure problems, such as that presented by Cho and Atluri (2002).

Numerous papers have been published about the various computations done for the AGARD wing (Bennet and Edward, 1998). A brief description of the existing methods and the features addressed in our model for the AGARD case is shown in Table 2. As can be seen from the table, our model incorporates all the key features that go into a CAE model viz., well-defined flow solver with moving mesh techniques and turbulence models, a separate structural solver and an interfacing technique that combines these two. Most of the models, until recently, used the same grid for both CFD and CSD computations. Recently, Liu et al (2000) developed a model for the AGARD wing, which uses separate grids with a corresponding interfacing between them and presented solutions using the Euler equations for flow module. We choose this as our benchmark model but we use the full Navier-Stokes solutions, neglecting compressibility effects, for our flow module. We present the interfacing techniques developed thus far using the linear time-invariant structure model for the AGARD wing model as well as the membrane model on a $\mu$AV wing.

**Table 1** : Table of a few existing aeroelastic models

| Author's Name | Description of work | Main Results |
|---|---|---|
| Cunningham, Batina, Bennett (1988) | • Computational scheme for transonic aeroelastic analysis to perform flutter analysis<br>• Flow: Transonic small disturbance formulation<br>• Structure: Lagrange Equations of motion based on the natural vibrational modes<br>• AGARD configuration with 45 deg sweep angle and M=0.338-1.141 | • Aerodynamic forces and flutter characteristics obtained using linear formulation compared well with experiment.<br>• Non-linear flutter results compared well with expt but not so with linear results<br>• Can treat configurations with arbitrary lifting surfaces |
| Schuster, Vadyak, Atta (1990) | • A 3-D flow solver coupled with linear static structural model to study aeroelastic response of aircraft<br>• Grid deflection method is used to update the grid after each time step<br>• CFD solver: ENS3D<br>• Swept, tapered wing with constant cross-section with M=0.9 and $\alpha$ = 9 deg was used<br>• Wing mesh: 92 x 32 x 32 points | • Aeroelastic analysis compared well with experiment with respect to pressure coefficient and twist<br>• Flexible wing/body configuration gave better results compared to rigid body configuration<br>• Separation on the upper surface was not predicted |
| Guruswamy Byun (1993)<br><br>Guruswamy Byun (1994) | • Compute aeroelasticity by direct coupling using time-integration method<br>• Fluid: Euler equations/N-S equations<br>• Structure: Plate finite elements<br>• Aerodynamic loads are transferred by bilinear interpolation and by virtual surface methods<br>• CFD grid (151 x 30 x 35)<br>• FEM grid (36 plate elements)<br>• Fighter type wing with M=0.854 and $\alpha$=1 deg. | • Validity of coupling plate elements with Euler equation<br>• Virtual surface method transfers loads more accurately than bilinear interpolation technique |
| Bhardwaj, Kapania, Reichenbach, Guruswamy (1998) | • Static aeroelastic solutions using a linear structural model.<br>• Flow solver: NASTD<br>• FEM solver: NASTRAN<br>F-18 wing with M=0.95 and $\alpha$=1 deg.<br>• CFD and CSD gird points are matched directly<br>• CFD grid (800,000 points)<br>• FEM grid (2000 nodes) | • Maximum deflection compares well with prev. analytical results<br>• Increased accuracy of direct finite element displacement data compared to modal analysis<br>• Aeroelastic coupling is not as efficient as a completely integrated scheme |
| Lewis and Smith (1998) | • External aeroelastic simulation for internal aerodynamics and shell structures<br>• Coupled set of structure and flow equations<br>• Predictor-corrector scheme for structural integration<br>• Solver used: ENS3DAE<br>• Tested on an engine liner to study flutter with M=0.7 in inner region and M=0.4 in the annular region | • Results showed the engine liner to be dynamically stable<br>• Inner flow mach no. had little effect on aeroelastic response<br>• Effect of pressure loadings on the shell structures were not considered in this method |

**Table 1** : (Cont.) Table of a few existing aeroealstic models

| Author's Name | Description of work | Main Results |
|---|---|---|
| Patil, Hodges, Cesnik (1999) | • Non-linear aeroelastic model for complete aircraft model for high AR wings<br>• Mixed variational formulation of beams in moving frames<br>• Finite-state airloads for deforming airfoils on fixed wings<br>• Linear and non-linear analysis were considered for comparative study<br>• Rigid and flexible wings were compared<br>• High-altitude, low-endurance aircraft is considered for performing tests | • Linear analysis produced almost identical results for frequencies of the beam for flutter calculations<br>• Flutter speed and freq was found to be less than that predicted by linear model<br>• Flight dynamics changed considerably for flexible wings<br>• The steady state solution and the frequency modes were affected by wing flexibility |
| Patil, Hodges (2000) | • Theoretical non-linear aeroelastic analysis of high AR wings to investigate effects of geometrical non-linearity<br>• Structural solver: nonlinear mixed variational formulation<br>• Aero solver: 3-D nonplanar double lattice theory<br>• Rigid slender wing with semi-span AR=16 and flexible wing with $\alpha$=10<br>• Grid: steady: 16 x 1; unsteady: 48 x 6 | • Structural nonlinearity, nonplanar geometry and 3-D effects have little effect on a rigid wing<br>• Nonplanar geometry and structural nonlinearity have negligible effect on flexible wings too<br>• A decrease in flutter speed with increase in wing loading was noted for flexible wings |
| Garcia, Guruswamy (1999) | • Model for coupled nonlinear beam FEM model with N-S solver for static aeroelastic analysis of high AR wings<br>• Flow solver: ARC3D fluids module of ENSAERO-WING code<br>• Structural code: NASTRAN<br>• Aeroelastic research wing (ARW-2) @ M=0.85 and $\alpha$=2 | • FEM results are accurate except for deflections which were smaller than modal results<br>• Nonlinear and linear beam models predicted similar pressure coefficient results<br>• Geometrical nonlinearity was found to be negligible |
| Soulaimani (2000) | • Methodology for non-linear computational aeroelasticity<br>• Flow solver: FEM based 3-D Euler and N-S eqns. For unstructured meshes with ALE formulation for moving grids<br>• Structure: Commercial FEM code<br>• Coupling: Partitioned solution procedures for time integration<br>• M=0.96 and $\alpha$=0 on a AGARD-445.6<br>• Unstructured Grid (84946 points) | • The FEM based scheme developed is found to be qualitatively similar to the finite volume schemes |
| Farhat and Lesoinne (2000) | • Serial and Parallel methodologies for nonlinear transient aeroelastic problems<br>• Arbitrary Lagrangian-Euler equations are incorporated into the unstructured flow solver<br>• Deforming mesh algorithm was used to enable grid movement<br>• M=0.901 on an AGARD wing | • Partitioned algorithms were found to be efficient than monolithic schemes |

**Table 1** : (Cont.) Table of a few existing aeroealstic models

| Author's Name | Description of work | Main Results |
|---|---|---|
| Rugonyi and Bathe (2001) | • Partitioned and Direct methodologies for fluid-structure interaction problems using FEM<br>• Flow: Finite element ALE formulation<br>• Structure: Lagrangian equations of motion<br>• Cases considered<br>– Pressure wave propagation in a tube<br>– Collapsing channel<br>– Fuel pumps and analysis of lamps | • Effectiveness of using FEM to obtain response of fluid flows and structures were enlightened<br>• Direct and Staggered methods were compared |

**Table 2** : Description of existing CAE methods for an AGARD wing

| Author | CFD solver | Deforming mesh algorithm | Structural solver | Interfacing technique |
|---|---|---|---|---|
| Cunningham et al (1988) | TSD | None | Modal Analysis | none |
| Robinson et al. (1991) | Euler | Spring analogy | Modal analysis | none |
| Lee-Rausch and Batina (1993) | Navier-Stokes | Spring analogy | Modal analysis | none |
| Soulaimani (2000) | FEM based | ALE formulation | Commercial code | none |
| Liu, et al. (2000) | Euler | TFI method | Modal equations of motion from FEA | Spline methods |
| Farhat and Lessoine (2000) | Unstructured Navier-Stokes | ALE formulation | Finite element based solver | Conservative method |
| Present approach | Full Navier-Stokes | TFI like method | Bernoulli-Euler beam equations | Linear interpolation extrapolation |

## 2 Numerical Procedure

### *2.1 Flow Solver*

A pressure-based numerical procedure presented (Shyy, 1994; Shyy et al. 1997) for curvilinear coordinates is adopted as the flow solver (STREAM). It solves the full Navier-Stokes equations for 3-D incompressible flows. The continuity equation and u-momentum equation are given below. The v and w-momentum equations can be written along similar lines.

$$\frac{\partial(J\rho)}{\partial t}+\frac{\partial(\rho U)}{\partial \xi}+\frac{\partial(\rho V)}{\partial \eta}+\frac{\partial(\rho W)}{\partial \gamma}=0 \tag{1}$$

$$\begin{aligned}
&\frac{\partial(J\rho u)}{\partial t}+\frac{\partial(\rho U u)}{\partial \xi}+\frac{\partial(\rho V u)}{\partial \eta}+\frac{\partial(\rho W u)}{\partial \gamma}\\
&=\frac{\partial}{\partial \xi}[\frac{\mu}{J}(q_{11}u_\xi+q_{12}u_\eta+q_{13}u_\gamma)]\\
&+\frac{\partial}{\partial \eta}[\frac{\mu}{J}(q_{21}u_\xi+q_{22}u_\eta+q_{23}u_\gamma)]\\
&+\frac{\partial}{\partial \gamma}[\frac{\mu}{J}(q_{31}u_\xi+q_{32}u_\eta+q_{33}u_\gamma)]\\
&-[\frac{\partial}{\partial \xi}(f_3 p)+\frac{\partial}{\partial \eta}(f_6 p)+\frac{\partial}{\partial \gamma}(f_9 p)]+G_1(\xi,\eta,\gamma).J
\end{aligned} \tag{2}$$

where $\xi$, $\eta$,$\gamma$ are time dependent curvilinear coordinates,

e.g., $\xi = \xi(x,y,z,t)$. Here, $u$ is the Cartesian velocity component, $p$ is the pressure, $\mu$ accounts for both laminar and turbulent viscosity. $U$, $V$, and $W$, are the contravariant velocity components and they read as follows:

$$U = f_{11}(u-\dot{x}) + f_{12}(v-\dot{y}) + f_{13}(w-\dot{z}) \quad (3)$$

$$V = f_{21}(u-\dot{x}) + f_{22}(v-\dot{y}) + f_{23}(w-\dot{z}) \quad (4)$$

$$W = f_{31}(u-\dot{x}) + f_{32}(v-\dot{y}) + f_{33}(w-\dot{z}) \quad (5)$$

where $f_{ij}, q_{ij}$ are the metrics of the conversion from Cartesian coordinates to curvilinear coordinates and $\dot{x}, \dot{y}$, and $\dot{z}$ are the grid velocities which are approximated by a first order backward time difference

$$\dot{x} = \frac{x - x^0}{\Delta t} \quad (6)$$

where $\Delta t$ is the fluid solver time step and the superscript refers to the previous time level. The determinant of the transformation matrix between Cartesian and curvilinear coordinates is given by

$$J = x_\xi y_\eta z_\zeta + x_\zeta y_\xi z_\eta + x_\eta y_\zeta z_\xi - x_\xi y_\zeta z_\xi - x_\zeta y_\eta z_\xi - x_\eta y_\xi z_\zeta \quad (7)$$

More detailed discussion about these equations can be found in Shyy (1994).

The solver incorporates many of the modern techniques for handling complex flow problems including multi-block methods and controlled numerical diffusion schemes for convection and pressure terms. A combined Cartesian-contravariant velocity formulation is adopted to facilitate a conservative, finite-volume formulation. The convection terms are treated using second-order upwind scheme, while the unsteady terms are treated using first order implicit Euler method. The remaining terms are treated using second-order central difference scheme. More details about the code can be found in Thakur and Wright (1999).

#### *2.1.1 Turbulence modeling*

We use the most widely employed two-equation model viz., the $\kappa - \varepsilon$ model for turbulent computations. Since the standard $\kappa - \varepsilon$ model is only valid in fully turbulent regions, it requires additional modeling near wall regions or in the no-slip regions. We use wall functions technique (Launder and Spalding, 1974) to model the near wall region. This technique uses the law of the wall as the constitutive relation between the velocity and the surface shear stress. The detailed formulation of the model can be found in Shyy et al. (1997).

#### *2.1.2 Updating Jacobian Values*

While formulating the above-mentioned flow solver for the moving boundary problem, we need to make sure that the geometric conservation law is satisfied. This was ensured by updating the Jacobian values after every time step. This satisfies the geometric conservation law given by

$$\frac{J - J^0}{\Delta t} + U|_w^e + V|_s^n + W|_b^t = 0 \quad (8)$$

where $J^0$ is the Jacobian from the previous time step and *e, w, n, s, t ,b* represent the six faces of the control volume which are named east, west, north, south, top and bottom respectively.

### *2.2 Linear Time-invariant Structural Model*

A general, linear, time-invariant structural model is used in the coupled CFD-CSD method. Thus, the equations of motion that govern the structural dynamics of the wing take the well-known form:

$$[M]\ddot{q}(t) + [C]\dot{q}(t) + [K]q(t) = Q(t) \quad (9)$$

where $[M]$ is the mass matrix, $[C]$ is the damping matrix, $[K]$ is the stiffness matrix, $Q(t)$ is a vector containing the generalized forces associated with aerodynamic loads, and $\mathbf{q}$ is a vector containing the generalized displacements. The structural solver integrates these equations of motion in time for one time step given the time step size, the pressures on structural nodes at the initial time for the time step, and the initial geometry of the wing.

The pressures are provided as scalar pressures located at structural grid points that were obtained and interpolated from a CFD calculation on a finer fluid grid. The geometry of the wing is defined in terms of the spatial global coordinates of each structural node, a list of pointers that show the relationship between nodes and surface elements, a list of pointers that show the relationship between surface elements and nodes, and a list of pointers that show the relationship between surface elements and super-elements.

Now, the structural model will be described in order to demonstrate how the structural solver integrates the equations of motion for a single time step. The scalar pressures, obtained from an interpolation of the pressures from a CFD calculation, are converted to pressure forces $(P_1, P_2, P_3)$ acting at each node of the structural grid. These pressure forces are the ones used to generate the aerodynamic loads ($Q_w$ and $Q_\theta$) on the wing, as illustrated by the equations:

$$\int_o^T Q(t)\,\delta q(t)\,dt = \int_0^T \int_S P \cdot \delta r dS dt \tag{10}$$

$$Q_w = \int_S P_3 N_w(y)\,dl dy \tag{11}$$

$$Q_\theta = \int_S [P_1(-\xi(y,l)\sin\theta(y) + \eta(y,l)\cos\theta(y)) - P_3(\xi(y,l)\cos\theta(y) + \eta(y,l)\sin\theta(y))]N_\theta(y)\,dl dy \tag{12}$$

Here, $N$'s are the shape functions, $y$ is the spanwise location and $l$ is the Chordwise location of the element.

Furthermore, the evaluation of the aerodynamic loads is accomplished by the use of single point quadrature over each surface element. Using these aerodynamic loads, the translation and twist of each super element is obtained with respect to the elastic axis of each super element. This is illustrated in Figure 1.

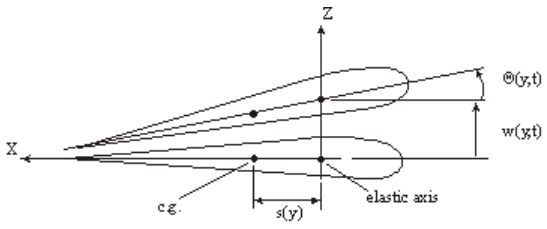


**Figure 1** : Displacements measured with respect to the Elastic Axis

The above model is used for the AGARD wing case where the cross-section is assumed to be rigid. However, for the membrane case, we cannot use the same model.

We formulate the membrane model based on the assumption that the membrane material considered obeys the hyperelastic Mooney-Rivin model. The Green-Lagrange strain tensor is used for the description of large strains. The dynamic response of such a membrane is described by a system of second-order time-dependent equations given by

$$[M]\ddot{D}(t) + F^{int} = F^{ext} \tag{13}$$

where $[M]$ is a positive definite mass matrix, $D(t)$ represents the nodal displacement vector, $F^{int}$ is the internal force and $F^{ext}$ is the external load. These equations are integrated in time using a second-order explicit scheme. An implicit method has also been developed. More details of the membrane model can be found in Lian et al. (2002).

### *2.3 Moving Grid Techniques*

For fluid/structure problems, we must account for grid movement along the deformed surface. Since the structure moves after every time step, we need to accommodate this movement in the CFD domain. This is usually done with some type of dynamics related mesh algorithm. For example, Robinson's (1991) spring analogy method deals with every grid point like a point mass connected with spring whose stiffness is inversely proportional to the length of the connecting points. More recently, to attack the complex multi-block case, Hartwich and Agrawal (1997), Wong et al. (2000), and Reuther et al. (1996) proposed their own methods. Although they have different forms, they all belong to the transfinite interpolation class. In our computation, we use Hartwich's method to deform the surface points and Reuther's perturbation method to regenerate the volume grid (Lian et al. 2001)

We use the master/slave concept to move the multi-block edges, where master nodes denote the list of all nodes on the moving boundary and slave nodes are all the nodes on the multi-block edges. The slave nodes are moved based on the deflection of the master nodes given by the following expression

$$\tilde{x}_s = x_s + \theta(\tilde{x}_m - x_m) \tag{14}$$

where the subscripts $m$ and $s$ represent master and slave, respectively, tilde $(\sim)$ indicates the new position and g$\theta$ is the decay function that controls the movement of the slave nodes, given by

$$\theta = \exp\{-\beta \min[FACTOR, dv/(\varepsilon + dm)]\} \tag{15}$$

where

$$dv = (x_v - x_m)^2 + (y_v - y_m)^2 + (z_v - z_m)^2 \tag{16}$$

$$dm = (\tilde{x}_m - x_m)^2 + (\tilde{y}_m - y_m)^2 + (\tilde{z}_m - z_m)^2 \tag{17}$$

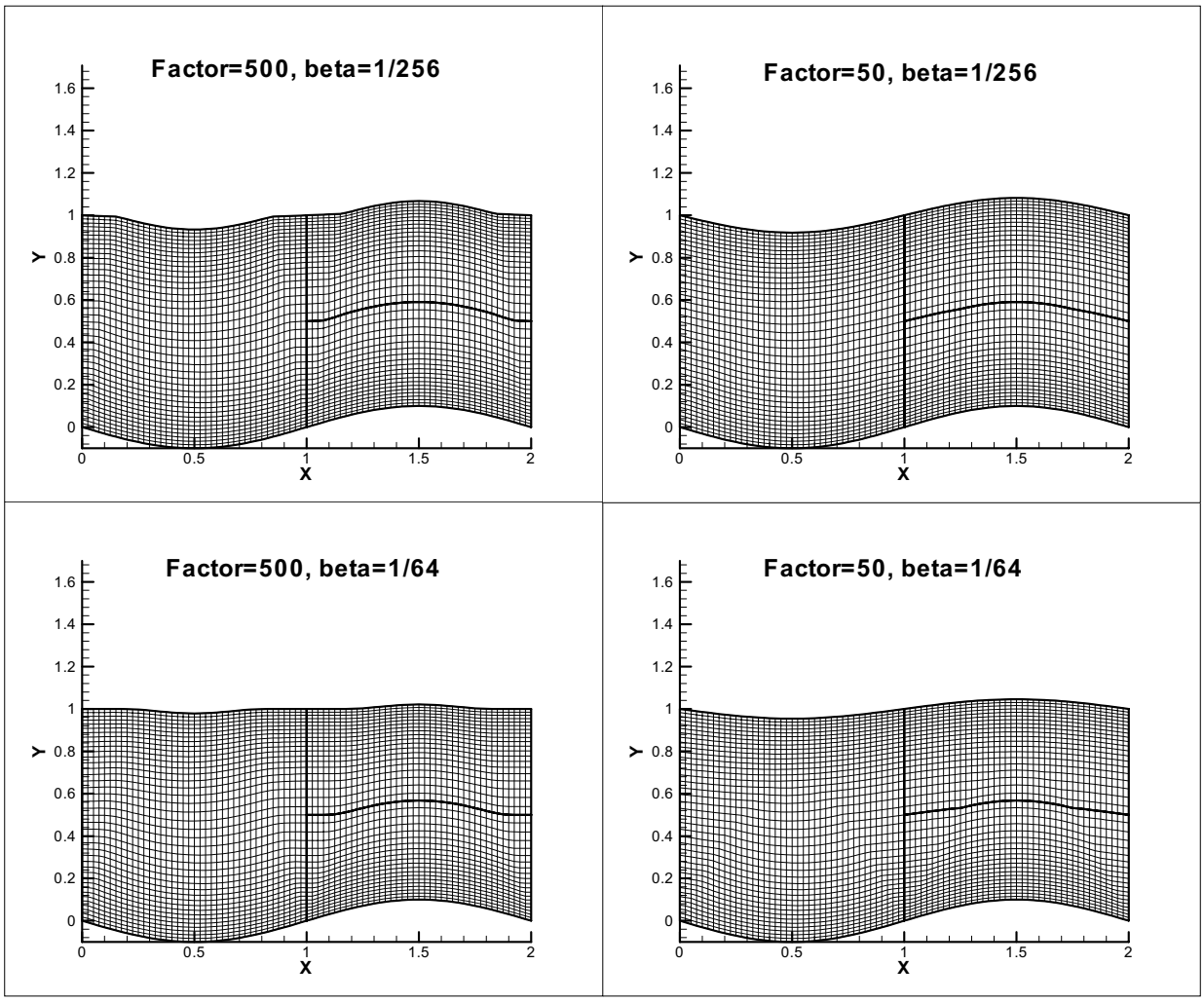


**Figure 2** : Figure depicting the effect of the 2 parameters, *FACTOR* and *beta* on the re-meshing.

*FACTOR* is some minimum value assigned to handle stiffness issues at far away grid points and $\varepsilon$ is an arbitrary small number to eliminate division by zero.

As can be seen from Eq. (15), the decay function itself is controlled by two parameters: $\beta$ and *FACTOR*. The second of these parameters matter only when *dv/dm* is greater than *FACTOR*. This is usually the case for small displacements i.e., when *dm* is very small compared to *dv* or for slave points away from the master nodes when *dv* becomes large compared to *dm*. The parameter, $\beta$ is used to control the nature of grid movement like a soft body or a rigid body. Lower value of $\beta$ correspond to higher value of $\theta$ implying a more rigid movement of blocks and higher value of $\beta$ correspond to lower value of $\theta$ implying a movement like a soft ball. The effect of these parameters on grid movement on a simple three-block grid is shown in Figure 2. The initial grid is just a rectangular domain and we treat the entire bottom surface as our moving boundary and give an arbitrary sinusoidal displacement to study the effects of these parameters.

Here, the master nodes are the nodes in the bottom surface of the domain, which we arbitrarily perturb. Note that all four figures have the same amount of perturbation. The slave nodes are all other block edge nodes that are in bold.

It can be seen from Fig. 2 that smaller values of both $\beta$ and *FACTOR* correspond to a movement like a rigid body. This is desirable near the boundary where there are sharp corners and the grid quality needs to be preserved. This will automatically take care of the value of $y^+$, which is an important factor while employing turbulent flow models with wall-functions.

### *2.4 Interfacing technique*

Developing an interfacing technique to interact back and forth between the fluid-structure models poses the greatest challenge in the field of CAE. The most difficult part of handling numerically the fluid/structure coupling stems from the fact that the structural equations are usually formulated with material (Lagrangian) coordinates, while the fluid equations are expressed using spatial (Eulerian) coordinates. As the two grids are different, one being a finite volume grid and other being a finite element grid, the two types of grid are not likely to coincide at the same points. The CFD grid is typically finer than the CSD grid as the flow properties are likely to change a lot in vicinities of large gradients. Hence, some kind of interpolation needs to be done between the grids to map the aerodynamic forces from the CFD grid onto the CSD grid. Along the same lines, once the displacement field is obtained from structure solver, data needs to be extrapolated from the CSD grid to the CFD grid. Several methods have been formulated thus far for the interfacing technique. Smith et al. (2000) provides an excellent review of a few interface methods.

We will now describe in detail the computational procedure used to perform fluid/structure interaction calculations.

## 3 Computational Procedure

In this section, we will discuss the various computational procedures associated with our aeroelastic computations and discuss at length the coupling issues that need to be addressed while formulating the model. The overall computational procedure can be divided into the following major steps.

- Geometry definition along with the necessary boundary conditions and initial condition.
- Perform CFD computation to obtain aerodynamic forces on the surface of the wing
- Interpolate aerodynamic forces onto the structural mesh
- Perform CSD computation to obtain the deformation of the geometry
- Extrapolate the deflection and twist to obtain the new CFD surface grid
- Re-mesh CFD grid based on the deformation obtained from the CSD calculations using the moving boundary module

These steps are repeated as we march in time. This procedure can be put in the form of a flow diagram as shown in Figure 3. Now we will take a closer look at the above-mentioned steps along with the grid generation details.

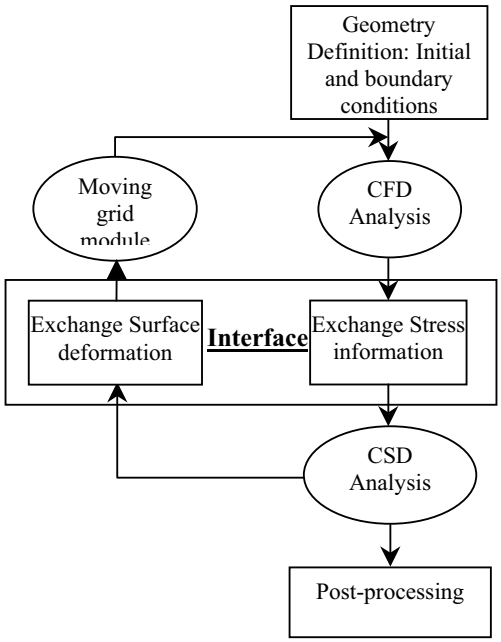


**Figure 3** : Computational Aeroelasticity analysis block diagram for time-domain analysis

### *3.1 Geometry definition*

We use the well-validated AGARD 445.6 wing (Yates, 1987) as our geometry for testing purposes. This is the first AGARD standard aeroelastic configuration (Yates et al. 1967). The AGARD 445.6 wing is a swept back wing with a quarter-chord sweep angle of $45^o$ with a NACA 65A004 airfoil cross-section. It has a panel aspect ratio of 1.65 and a taper ratio of 0.66. The root chord of this model was 1.833 feet and it has a semi-span of 2.5 feet. The wing tested at NASA Langley was a semi-span, wall-mounted model made with laminated mahogany. A schematic of the AGARD wing is shown in Figure 4.

We will now look at the computational grids used by the fluid and structure solvers.

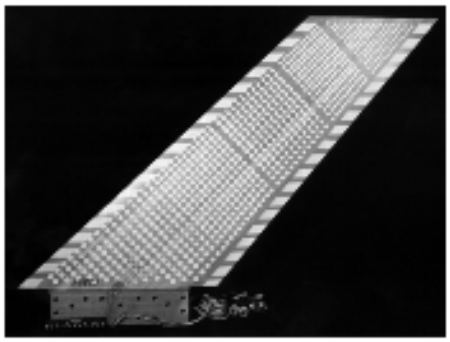

**Figure 4** : Schematic of teh AGARD 445.6 wing used in the wind tunnel (Yates, 1967)

### *3.2 Computational Grids*

#### *3.2.1 CFD grid*

We generate a CFD mesh around an AGARD 445.6 wing by placing the wing in the middle of the computational domain, which has dimensions of 10c x 5c x 5c as shown in Figure 5. Here c is the chord length at the root of the wing. The geometry could be generated by using the CAD module of any commercial mesh-generating softwares such as ICEMCFD or PATRAN, the latter being easier for simple geometries. We used PATRAN for generating the wing geometry along with the computational domain and ICEMCFD was used to generate the multi-block CFD grid containing 10 blocks. Since this is a very thin wing, care must be taken while generating mesh around the wing tip and trailing edge to avoid any negative Jacobian values. As a first step, we use a mesh which has 4838 points distributed over the wing surface (118 points in the chordwise direction and 41 points in the spanwise direction).The entire CFD domain has a total of 322,622 points. The CFD surface grid along with the meshing system at the leading and trailing edges are shown in Figure 6 for clarity.

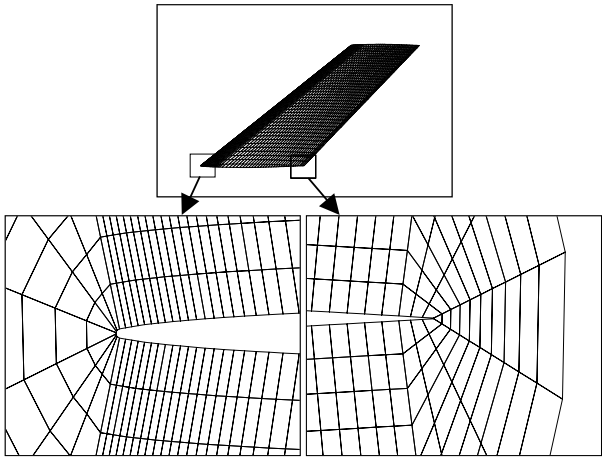

**Figure 6** : CFD surface grid along with grid distributions at the leading and trailing edges.

#### *3.2.2 CSD grid*

For the structure solver, we need to generate grid only on the surface as the structure only inside the wing matters for computational purposes. Since we use linear beam elements, this eliminates generating mesh inside the wing. The finite element surface mesh is generated using PATRAN and has 2501 points on the surface (61 along

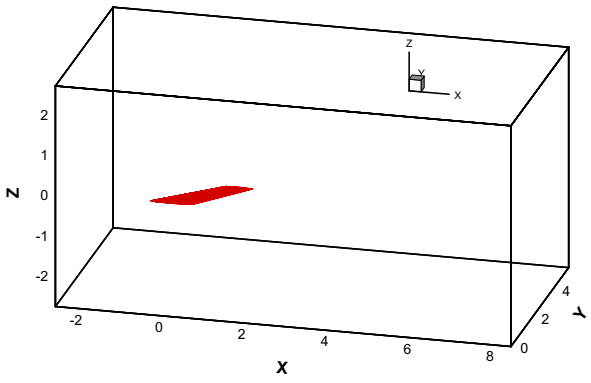


**Figure 5** : Overview of the CFD computational domain

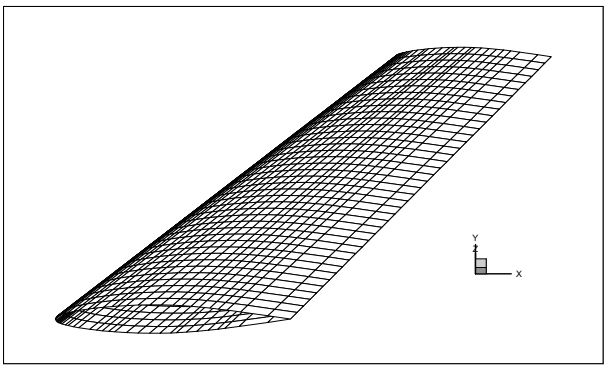

**Figure 7** : Schematic of the FEM grid on the AGARD wing

the chordwise direction and 41 along the spanwise direction) of the wing. The grid is shown in Figure 7. As can be seen, it contains far less points than that of CFD mesh which clarifies the need for an interfacing technique.

### *3.3 Coupling procedure*

Having generated the necessary computational grids, our focus shifts towards specifying the boundary and initial conditions necessary for starting the computations. We will now discuss at length how the different computational issues are tackled.

First, we run the flow solver based on the initial guess to obtain surface pressures on the CFD grid of the wing. These scalar pressures are then interpolated onto the CSD grid by employing a bilinear interpolation procedure. This is done by treating the top and bottom surface of the wing as two-dimensional surfaces and mapping the pressures from the CFD surface grid to the respective CSD surface grid. This is done by locating the four CFD grid points engulfing a given CSD grid point and employing a straightforward interpolation procedure. This is demonstrated via Figure 8.

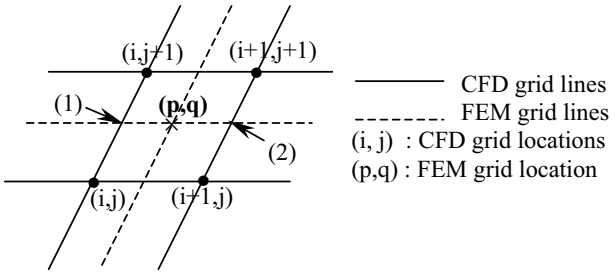


**Figure 8** : Schematic to demonstrate interpolation technique

Once we locate the points engulfing (p, q), we calculate intermediate pressures at points (1) and (2) by a linear interpolation procedure and these intermediate pressures are further used to evaluate pressure at point (p, q) by linear interpolation. Such a scheme gives an order of accuracy between one and two.

Now that we have obtained surface pressure distribution on the CSD grid, we now have to convert these scalar pressures into pressure forces by computing the unit normal and surface area for each element. We divide the CSD grid shown in Figure 7 into ten strips or super elements or beam elements along the spanwise direction. Each super element has 4 surface elements in the spanwise direction and 60 surface elements in the chordwise direction as shown in Figure 9. The net pressure force for each super element was then calculated which acts as the loading for solving the equations of motion. The mass and stiffness matrix for the structure are obtained from full NASTRAN models. Since the structural solver is limited by a critical time step size, which takes a value of 1.8 x $10^{-6}$, we had to run the structure solver a number of times in order to make it synchronize with the flow solver, the time step for which was taken as 9 x $10^{-4}$, as the flow solver uses a fully implicit method.

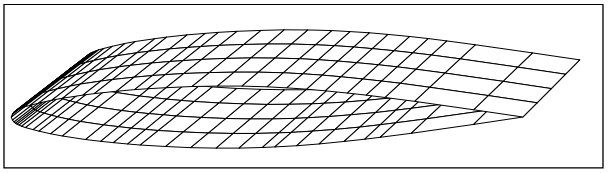

**Figure 9** : Schematic of a super element: Portion of the entire structure

By modeling the structure as a one-dimensional beam, we are assuming that the cross-section of the wing remains unchanged or rigid. Thus we determine the motion of the CFD grid knowing the motion of the structure by assuming a rigid link connecting each CFD grid point to the beam element. The links are assumed to be perpendicular to the elastic axis as shown in Figure 10.

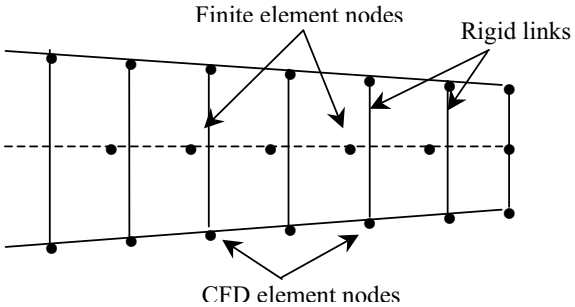


**Figure 10** : Sample CFD mesh superimposed on the discretized beam structure

We define the state of the beam at any point along the spanwise direction as $w_s = \{w_1\ w_2\ w_3 \mid \theta_1\ \theta_2\ \theta_3\}^T$,
where $w$ represents the deflection and $\theta$ the twist at each spanwise section and subscripts 1, 2, 3 denote displacements in the x, y and z directions respectively. For our

case, we assume no deflection in the x and y directions and no rotation about the x and z axes. In other words, the deflection of a CFD grid point P can be written as

$$w_P = w_{P_T} + w_{P_R} \tag{18}$$

where $w_{P_T}$ is the translation component and $w_{P_R}$ is the rotational component. The translation and rotation component corresponding to CFD spanwise grid locations are obtained by performing a linear interpolation using the CSD spanwise grid points.

Having obtained the new CFD surface grid from the beam displacements, we now need to regenerate the entire CFD domain by making use of the moving mesh module. The new CFD surface grid acts as the source of perturbation needed to enable re-meshing as explained earlier. Once we have the new CFD grid, we need to ensure geometric conservation law, which was done by calculating Jacobian values of the new grid based on Eq (8) and not Eq. (7). This entire procedure is then repeated for subsequent time steps to arrive at desired aeroelastic results.

## 4 Results and Discussion

We now present the results to demonstrate the fluid-structure interaction in two different scenarios. First, we consider the AGARD 445.6 wing to demonstrate the fluid-structure interaction on a 3-D wing, which undergoes bending and torsion wherein the cross-section moves like a rigid body. Secondly we demonstrate the interaction between the fluid and flexible structure on a flexible membrane wing used in micro air vehicles.

### *4.1 AGARD 445.6 wing in turbulent fluid flow*

In our ongoing effort to develop a complete CAE model, we have made advances thus far to validate our code for performing the necessary interfacing technique. We carry out an unsteady, viscous, turbulent flow calculation on the AGARD wing with a Reynolds number of 366,000, which is in agreement with the experimental setup. We use a time step size of 0.0018 for the flow solver and a step size of $1.8\text{x}10^{-6}$for the structure solver, which is $1/1000^{th}$ of the flow time step used. This choice of structure time step arises from the fact that an explicit central difference scheme is used for the structural solver. In order to ensure stability, the time step, $\Delta$t, must be smaller than a critical time step, $\Delta t_{cr}$, defined to be $T/\pi$ (Bathe, 1982) where T is the period of the largest natural frequency of the structure. Using the mass and stiffness matrices generated for the tested model, the highest frequency is found to be $1.68\text{x}10^{5}$ Hz. The critical time step for this model is found to be $1.90\text{x}10^{-6}$seconds. We iterate the structure solver a thousand times for every fluid time step in order to make it synchronize with the fluid time step.

We ran the code for a number of time steps, updating the mesh after every time step using the deforming mesh algorithm. We assigned values of 1/256 and 500 for $\beta$ and *FACTOR* respectively to the parameters associated with the moving mesh module. Figure 11 shows the deflection of the wing in the spanwise direction at four different time instances with increasing time as indicated by the arrowhead. Displacement contours on the surface of the wing at these corresponding time instances are also shown in Figure 12.

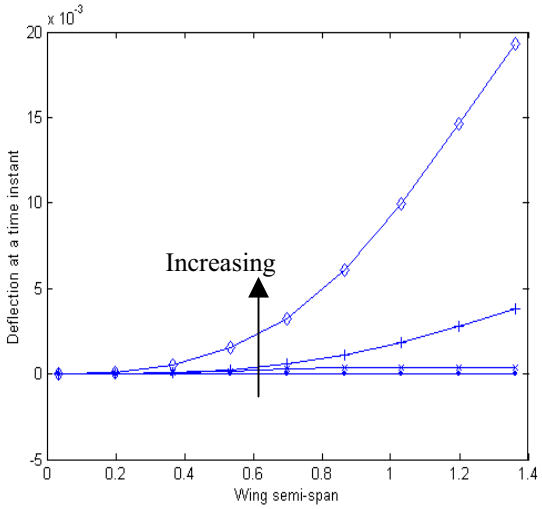


**Figure 11** : Deflection of the wing in the spanwise direction at four different time instants

As can be seen from the figure, the deflection at the wing tip increases with increasing time. A magnified three-dimensional wing shape to clarify the dominance of two bending modes is shown in Figure 13 (a) and (b). Figure 13 (a) depicts the transient response at t=0.012 in which the response is dominated by the second bending mode whereas Figure 13 (b) shows the transient response at t=0.043 which illustrates the predominance of first bending mode. The pressure contours at the top surface of the wing is shown in Figure 14. Corresponding pressure

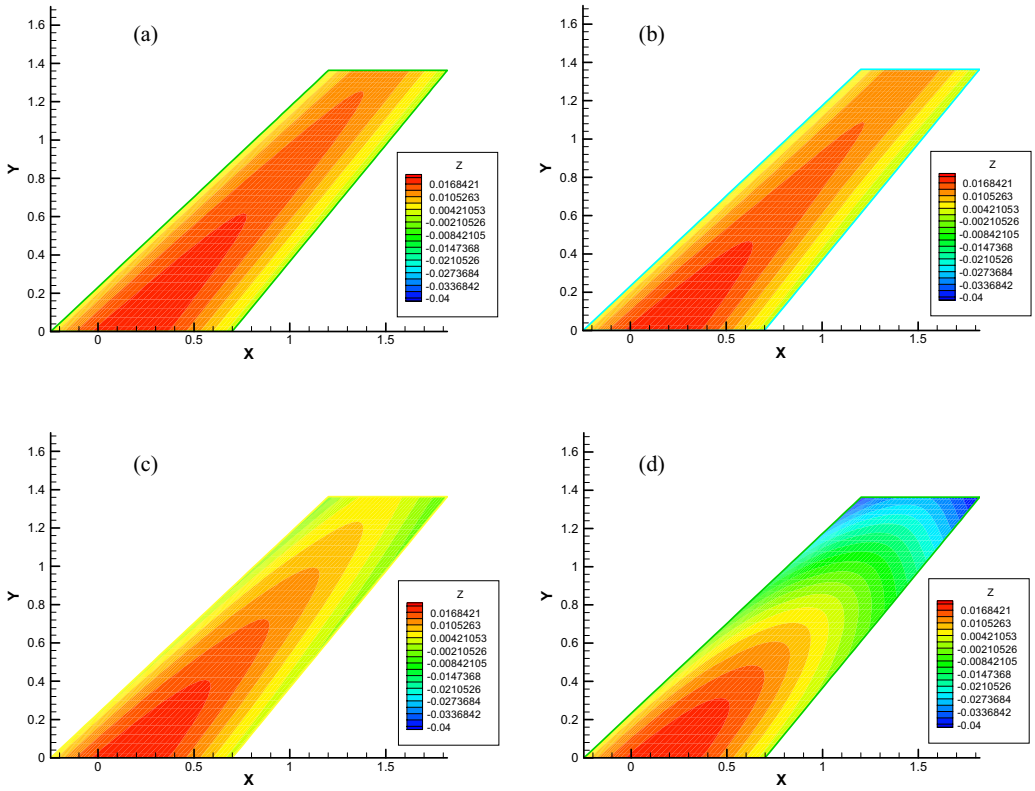


**Figure 12** : Displacement contours on the AGARD wing at the corresponding time instants shown in Figure 11, (a) through (d) represent increasing time.

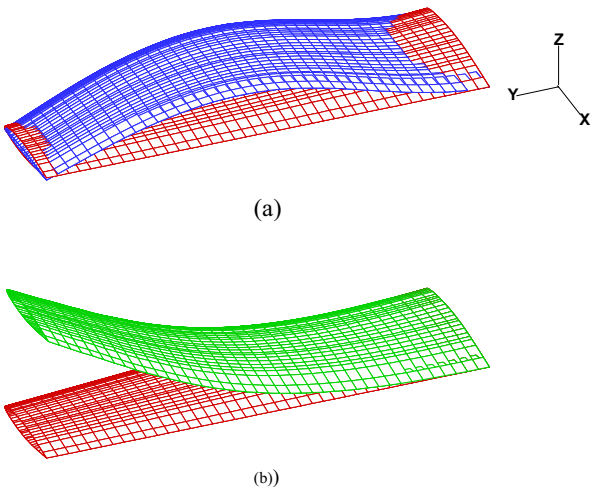


**Figure 13** : Magnified 3-D shape of the wing at two different time instants demonstrating the transient response (a) at t=0.012 s depicting dominance of second bending and (b) at t=0.043 s depicting dominance of first bending.

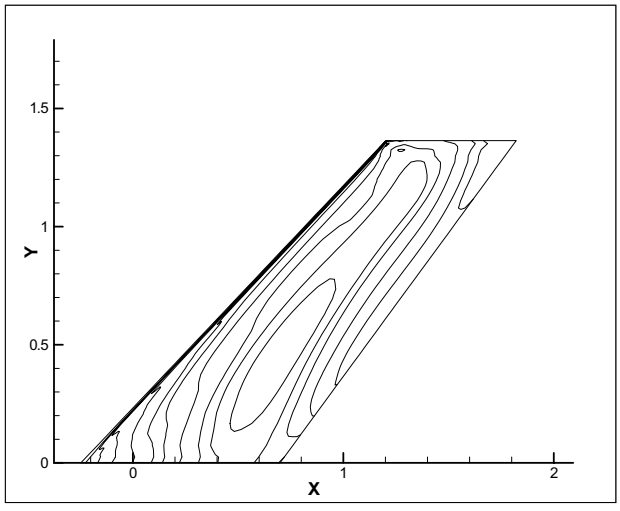


**Figure 14** : Surface pressure contours on the AGARD wing

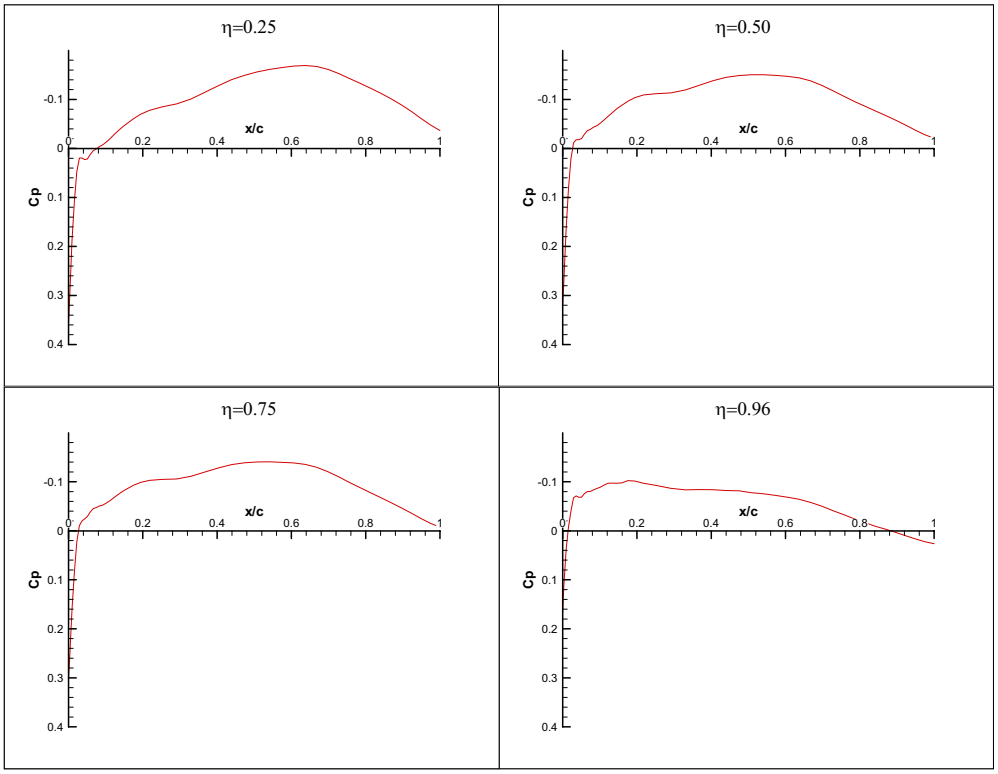


**Figure 15** : Pressure coefficient distribution at different spanwise locations (25%, 50%, 75%, and 96%) on the top surface of the wing

coefficients at different spanwise locations on the top surface of the wing are also shown in Figure 15. This is in good agreement with Lee-Rausch and Batina (1993) for the given turbulent Reynolds number.

### *4.2 Membrane Wing in a laminar fluid flow*

Beside the fluid and rigid structure interaction, we also investigate the interaction between a flexible structure and its surrounding fluid flow. In our computations we study the performance of a flexible membrane wing in a steady fluid flow. The computational domain for the membrane wing is shown in Figure 16. The membrane wing has a chord length of 13.7 cm and a span of 15 cm. There are three carbon fibers per semi-span of the wing to support the membrane. The overall skeleton of the wing is shown in Figure 17.

The shaded region in the figure is assumed to be rigid for our computation. Typically an $\mu$AV flies at an angle of attack of $6^o$ with a speed of 10 m/s. The resulting chord Reynolds number is $9x10^4$. To investigate the mutual interaction between the flexible structure and the fluid, a dynamic membrane model was proposed by

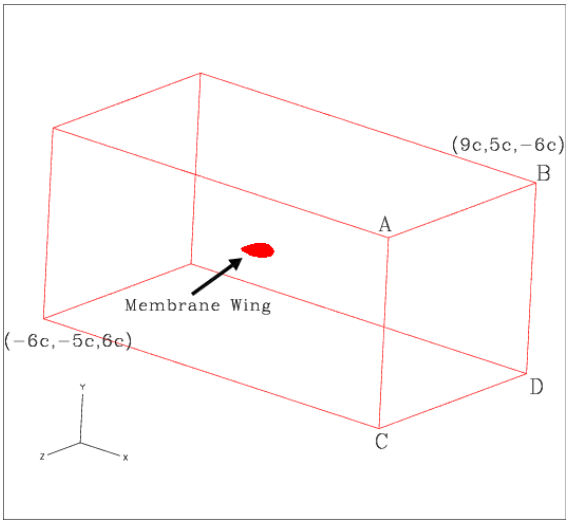


**Figure 16** : Computational domain for membrane wing

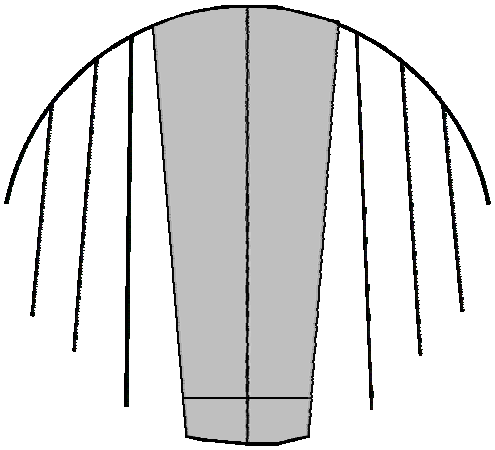

**Figure 17** : Skeleton of the membrane wing showing the carbon fibers

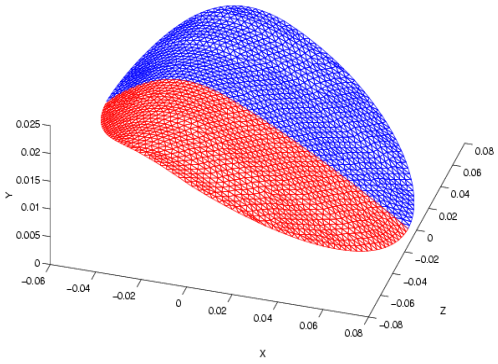


**Figure 18** : Unstructured finite element grid for the membrane wing

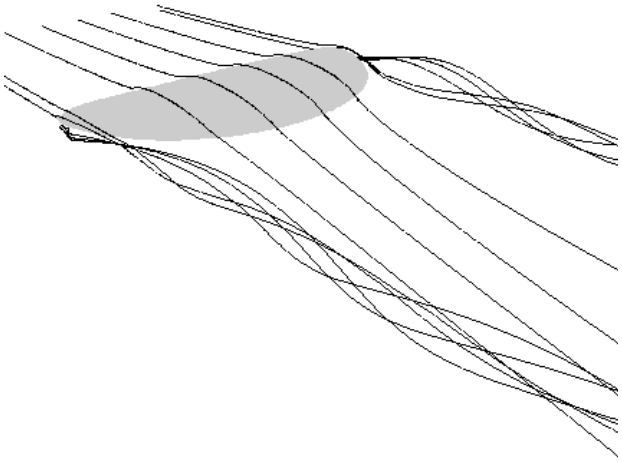

**Figure 19** : Streamlines around the rigid wing at angle of attack 6°

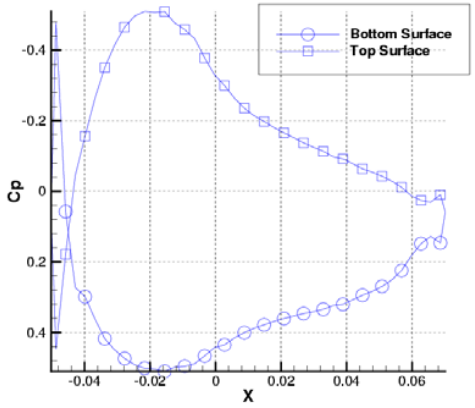


**Figure 20** : Pressure distribution along the streamwise direction at t=0.22

Lian et al (2002). This model can handle relatively large displacement of the membrane wing. We use finite element method for the membrane wing shape change and a pressure-based flow solver to calculate the aerodynamic load on the membrane wing. An unstructured mesh, generated for the FEM model, is shown in Figure 18. It has 1030 triangular elements and 1098 nodes on the semi-span of the wing. Streamlines demonstrating the tip vortex are shown in Figure 19. It is interesting to see that the pressure at the leading edge, at this angle of attack, is larger at the top than that at bottom as can be seen in Figure 20. This will eventually cause a kink at the leading edge of the membrane wing. Even in the steady fluid flow, the membrane wing demonstrates a self-excited vibration. Due to the nonlinear dynamic behavior of the membrane, the membrane vibrates with uneven frequencies. We show the displacement of the trailing edge in Figure 21 at different time instances. The vertical solid lines represent the position of the carbon fibers in the wing which we fix in our computations.

## 5 Summary and Conclusions

The present work is motivated in part by our interest in developing a comprehensive capability to account for fluid and structure interactions, and to facilitate a computation-based optimization capability for problems involving such issues. For fluid and structure interaction aspects, we have offered a detailed account of our studies and other representative studies. For optimization as-

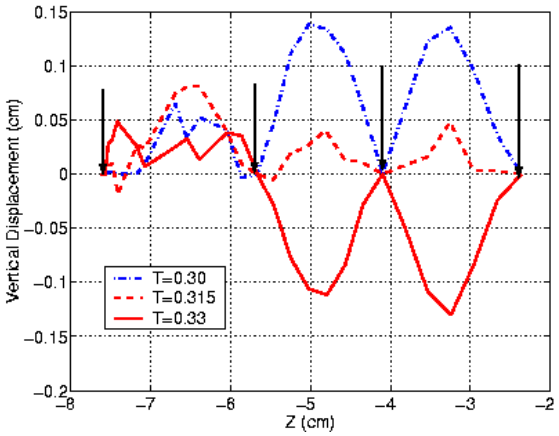


**Figure 21** : Trailing edge displacement of the membrane wing at different time steps

pects, we cite recent works by Okumura and Kawahara (2000) and Levin and Shyy (2001) for further details.

Two kinds of fluid-structure interaction, one between rigid wing cross-section structure and fluid and other between flexible structure and fluid, were studied. The rigid structure-fluid interaction was demonstrated using the AGARD wing model whereas the flexible structure-fluid interaction was studied using the membrane wing model of a micro air vehicle. The algorithm used for the aeroelastic computations incorporated a deforming mesh algorithm and a structure solver in addition to the existing pressure-based flow solver.

Unsteady aeroelastic computations were performed for both laminar and turbulent flows. Two different mode shapes are shown for the AGARD wing model. The pressure coefficient plots for both kinds of flows illustrated the cross over of lines near the leading edge which eventually lead to a kink in the membrane shape but this was not encountered for the AGARD wing as we assumed the cross-section to be rigid. Work is in progress to include compressibility effects in the flow code and to incorporate history dependent structural effects including hysteresis and load stiffening in the structural model.

**Acknowledgement:** The work reported has been supported by AFOSR, Dr. Len Sakell program monitor.

## References

**Atluri, S.N. and Shen, S.** (2002a) The Meshless local Petrov-Galerkin (MLPG) Method, Tech Sciences Press, Encino, CA.

**Atluri, S.N and Shen,S.** (2002b) The Meshless local Petrov-Galerkin (MLPG) Method: A Simple & Less-Costly Alternative to the Finite Element & Boundray Element Method, CMES: Computer Modeling in Engineering & Sciences, Volume 3, No. 1, pp11-52.

**Bathe, Klaus-Jurgen** (1982) Finite Element Procedures in Engineering Analysis, Prentice-hall inc., New Jersey.

**Bennett, R. M. and Edwards, J. W.** (1998) An Overview of Recent Developments in Computational Aeroelasticity, *AIAA-98-2421*.

**Bhardwaj, M. K., Kapania, K., Reichenbach, E. and Guruswamy, G. P.** (1998) Computational Fluid Dynamics/Computational Structural Dynamics Interaction Methodology for Aircraft Wings, *AIAA J.*, v. 36, n.12, pp. 2179-2186.

**Cho J.Y. and Atluri S.N.** (2001) Analysis of shear flexible beams, using the meshless local Petrov-Galerkin method, based on a locking-free formulation, *Engineering computations*, v. 18, pp. 215-240.

**Cunningham. H. J., Batina, J. T. and Bennett, R. M.** (1988) Modern Wing Flutter Analysis by Computational Fluid Dynamics Methods, *J. Aircraft*, v. 25, n. 10, pp. 962-968.

**Farhat, C. and Lesoinne, M.** (2000) Two efficient staggered algorithms for the serial and parallel solution of three-dimensional nonlinear transient aeroelastic problems, *Comput. Methods Appl. Mech. Engg.*, n. 182, pp. 499-515.

**Garica, J. A. and Guruswamy, G. P.** (1999) Aeroelastic analysis of Transonic Wings Using Navier_stokes Equations and a Nonlinear Beam Finite Element Model, *AIAA-99-1215*

**Guruswamy, G. P. and Byun, C.** (1994) Direct Coupling of Euler Flow Equations with Plate Finite Element Structures, *AIAA J.*, v. 33, n. 2, pp. 375-377.

**Guruswamy, G. P. and Byun, C.** (1993) Fluid-Structure Interactions Using Navier_stokes Flow equations Coupled with Shell Finite Element Structures, *AIAA-93-3087*.

**Hartwich, P. M., and Agrawal, S.** (1997) Method for Perturbing Multi-block Patched Grids in Aeroelastic and Design Optimization Applications, *AIAA Paper 97-2038*.

**Ifju, P., Jenkins, D., Ettinger, S., Lian, Y., and Shyy, W.** (2002), Flexible-Wing-Based Micro Air Vehicles,

40th AIAA Aerospace Sciences Meeting & Exhibit, AIAA. Paper 2002-0705.

**Launder, B. E. and Spalding, D. B.** (1974) The Numerical Computations of Turbulent Flows, *Comp. Meth. Appl. Mech. Engg.*, v. 3, pp. 269-289.

**Lee-Rausch, E. M. and Batina, J. T.** (1993) Calculations of AGARD Wing 445.6 Flutter using Navier-Stokes Aerodynamics, *AIAA-93-3476.*

**Levin, O. and Shyy, W.** (2001) Optimization of a Flexible Low Reynolds Number Airfoil, *Computer Modeling in Engineering & Sciences*, v. 2, pp.523-536.

**Lewis, A. P. and Smith, M. J.** (1998) Extension of a Euler/Navier-Stokes Aeroelastic Analysis Method for Shell Structures, *AIAA-98-2656*.

**Li, S. and Liu, W.K.** (2001) Meshless and Particle Methods and Their Applications, *Applied Mechanics Reviews*, v. 55, n. 1, pp. 1-34.

**Lian, Y., Steen, J., Trygg-Wilander, M., and Shyy, W.** (2001) Low Reynolds Number Turbulent Flows around a Dynamically Shaped Airfoil, *AIAA-2001-2723*.

**Lian, Y., Shyy, W., Ifju, P., and Verron, E.** (2002) A Computational Model for Coupled Membrane-Fluid Dynamics, *AIAA-2002-2972*

**Liu, F., Cai, J., Zhu, Y., Tsai, H. M. and Wong, A. S. F.** (2000) Calculation of Wing Flutter by a Coupled Fluid-Structure Method, *J. Aircraft*, v. 38, n. 2, pp. 334-342.

**Okumura, H. and Kawahara, M.** (2000): Shape Optimization of Body Located in Incompressible Navier-Stokes Flow Based on Optimal Control Theory, *Computer Modeling in Engineering & Sciences*, v. 1, pp. 71-78.

**Patil, M. J., Hodges, D. H. and Cesnik, C. E. S.** (1999) Nonlinear Aeroelastic and Flight Dynamics of High-Altitude Long-Endurance aircraft, *AIAA-99-1470*.

**Patil, M. J. and Hodges, D. H.** (2000) On the Importance of Aerodynamic and Structural Geometrical Nonlinearities in Aeroelastic Behavior of High-Aspect Ratio Wings, *AIAA-00-1448*.

**Reuther, J., Jameson, A., Farmer, J., Martinelli, L., and Saunders, D.** (1996) Aerodynamics Shape Optimization of Complex Aircraft Configurations via an Adjoint Formulation, *AIAA Paper 96-0094*.

**Robinson, B. A., Batina, J. T. and Yang, H. T. Y.** (1991) Aeroelastic Analysis of Wings Using the Euler Equations with a Deforming Mesh, *J. Aircraft*, v. 28, n. 11, pp. 781-788.

**Rugonyi, S. and Bathe, K. J.** (2001) On Finite Element Analysis of Fluid Flows Fully Coupled with Structural Interactions, *Computer Modeling in Engineering Sciences*, v. 2, n. 2, pp. 195-212.

**Schuster, D. M., Vadyak, J. and Atta, E.** (1990) Static Aeroelastic Analysis of Fighter Aircraft Using a Three-*Dimensional* Navier-Stokes Algorithm, *J. Aircraft*, v. 27, n. 9, pp. 820-825.

**Shyy, W.** (1994) "Computational Modeling for Fluid Flow and Interfacial Transport", Elsevier, Amsterdam.

**Shyy, W., Thakur, S.S., Ouyang, H., Liu, J. and Blosch, E.** (1997) "Computational techniques for Complex Transport Phenomena", Cambridge University Press, New York.

**Smith, M. J., Hodges, D. H. and Cesnik, C. E. S.**, (2000) Evaluation of computational Algorithms Suitable for Fluid-Structure Interactions, *J. Aircraft*, v. 37, n. 2, pp. 282-294.

**Soulaimani, A.**, (2000) A Finite Element Based Methodology For Computational Nonlinear Aeroelasticity, *AIAA-2000-2335*.

**Thakur, S. and Wright, J.** (1999) "STREAM: A Computational Fluid Dynamics and Heat Transfer Code for Complex Geometries. Part 1: Theory. Part 2: User's Guide" Streamline Numerics, Inc., Gainesville, Florida.

**Tsai, H.M., Wong, A.S.F., Cai, J., Zhu, Y. and Liu, F.** (2001) Unsteady Flow Calculations with a Multi-Block Moving Mesh Algorithm, *AIAA J.*, v. 39, n. 6, pp.1021-1029.

**Yates, E. C., Jr.**, (1987) AGARD *Standard Aeroelastic Configuration for Dynamic Response, Candidate Configuration I.-Wing 445.6*, NASA TM 100492.